Available online at www.sciencedirect.com
ScienceDirect
Trans. Nonferrous Met. Soc. China 29(2019) 2047−2055
Transactions of Nonferrous Metals Society of China
www.tnmsc.cn

Precipitate evolution in Mg−7Gd−3Y−1Nd−1Zn−0.5Zr alloy during isothermal ageing at 240 °C

Wei LIU[1,2], Zhi-wei DU[1, 2, 3], Ting LI[1, 2, 3], Kui ZHANG[4], Xiao-lei HAN[1,2], Yong-gang PENG[1,2], Jing ZHANG[1,2], Jia-wei YUAN[4], Shu-feng LIU[1,2], Zheng PANG[1,2]

1. Guobiao (Beijing) Testing & Certification Co., Ltd., Beijing 100088, China;
2. National Center of Analysis and Testing for Nonferrous Metals and Electronic Materials, GRINM Group Co., Ltd., Beijing 100088, China;
3. China United Test & Certification Co., Ltd., Beijing 100088, China;
4. State Key Laboratory of Non-ferrous Metals & Processes, GRIMAT Engineering Institute Co., Ltd., Beijing 101407, China

Received 7 January 2019; accepted 26 April 2019

Abstract: The morphology and crystal structure of the precipitates in Mg−7Gd−3Y−1Nd−1Zn−0.5Zr alloy during isothermal ageing at 240 °C were investigated using transmission electron microscopy (TEM) and high-angle annular dark-field scanning transmission electron microscopy (HAADF-STEM). After under-ageing for 2 h, the precipitates in the alloy are ordered solute clusters with rare earth atomic columns exhibiting hexagonal ring structure, zigzag GP zones and β' in its early formation. After peak-ageing for 18 h, the precipitates are mainly β' and new rod-like β'_p accompanied with β'. After over-ageing for 100 h, the precipitates are β', β_1, long-period stacking ordered (LPSO) building block known as γ' and 14H-LPSO. β' has the three-dimensional shape of convex lens with smaller length-to-width ratio viewed along $\langle 0001 \rangle_\alpha$ than that in the EW75 alloy. The excellent thermal stability of this alloy can be attributed to the γ' and 14H-LPSO retarding the growth of β' and β_1, low diffusion rate of rare earth atoms and physical character of β' and β_1.

Key words: magnesium alloy; ageing; precipitate; long-period stacking ordered (LPSO) phase

1 Introduction

The addition of rare-earth (RE) elements can significantly provide excellent performance for the magnesium alloy used in aerospace and automotive industries [1−3]. It has been reported that the Mg−Gd−Y alloys exhibit high specific strength, excellent mechanical properties and creep resistance [4−7]. In recent years, high strength and good ductility have been found in Mg−Gd−Y−Nd−Zn−Zr alloys with long-period stacking ordered (LPSO) precipitates [8].

The addition of different solution elements will result in different precipitation sequences. In binary alloys like Mg−Gd, the precipitation sequence during isothermal ageing treatment was proposed as α-Mg super-saturated solid solution (SSSS) → β'' (DO_{19}) → β' (BCO) → β (FCC, Mg_5Gd) [9]. Metastable precipitate β'' has a DO_{19} crystal structure (hexagonal, a=0.64 nm and c=0.52 nm). Metastable precipitate β' has a base-centered orthorhombic structure (BCO, a=0.64 nm, b=2.22 nm and c=0.52 nm). Stable β precipitate has a face-centered cubic crystal structure (FCC, a=2.22 nm), while another metastable precipitate β_1 is found between β' and β precipitates with a face-centered cubic crystal structure (FCC, a=0.740 nm) [10−12].

In the aging process, the addition of Zn in Mg−7Y−4Gd−0.5Zn−0.4Zr and $Mg_{96.5}Zn_1Gd_{2.5}$ (at.%) alloys produces another precipitation sequence: α-Mg (SSSS) → 14H-long-period stocking ordered (LPSO) [13,14]. Moreover, the addition of Zn to Mg−Y alloys contributes to the formation of stacking faults (SF)

Foundation item: Projects (51871195, 51501015) supported by the National Natural Science Foundation of China; Project (TC170A5SU-1) supported by Ministry of Industry and Information Technology, China
Corresponding author: Zhi-wei DU, Tel: +86-10-82241349, E-mail: duzhiwei@gbtcgroup.com; Kui ZHANG, Tel: +86-10-82241168, E-mail: zhkui@grinm.com
DOI: 10.1016/S1003-6326(19)65111-3

which can impede the movement of dislocations [15]. In addition, the addition of Zn causes the precipitation of a 14H-LPSO phase at grain boundaries and within grains. And the 14H-LPSO phase improves the deformation plasticity by reducing the strength of the Mg−2.0Gd−1.2Y−0.2Zr (at.%) alloy [16].

The EW75 (Mg−7Gd−5Y−1Nd−0.5Zr) alloy with excellent strength at both room and elevated temperature has been developed by our team [17]. In the peak aging stage, the main precipitates are β' precipitates. In order to improve the elongation of EW75 alloy, the composition optimization with Zn addition has been studied to obtain both LPSO structure and β-type precipitates. The ultimate tensile strength (UTS), yield strength (YS) and elongation of the peak-aged Mg−7Gd−3Y−1Nd−1Zn−0.5Zr alloy have reached 400 MPa, 351 MPa and 7% [8,18], respectively. The elongation is larger than that of EW75; however, the micro-mechanism is unclear.

Although there are many studies on the microstructure and properties of Mg−RE−Zn alloys, the aging precipitation behavior is still controversial. This work aims at clarifying the precipitate evolution in a Mg−7Gd−3Y−1Nd−1Zn−0.5Zr alloy during isothermal ageing at 240 °C. The morphology, size and crystal structure of the precipitates in ageing stage were investigated using transmission electron microscopy (TEM) and high-angle annular dark-field scanning transmission electron microscopy (HAADF-STEM).

2 Experimental

The Mg−7Gd−3Y−1Nd−1Zn−0.5Zr alloy was melted in an electrical resistance furnace. Based on the previous experiments, in order to prevent overheating of as-cast eutectic structure, one-step solution treatment (525 °C, 48 h) was implemented. After the solution treatment, the samples were quenched in warm water at 30 °C followed by ageing at 240 °C. The hardness of the samples was measured by Brinell hardness tester with a load of 613 N and dwelling time of 25 s. The sample discs (3 mm in diameter) were ground to a thickness of 0.05 mm and twin-jet electro-polished in a solution of 3 vol.% perchloric acid and 97 vol.% ethanol, at temperature from −40 to −50 °C with the current of about 15 mA. The HAADF-STEM images of the precipitates in the under-ageing stage were analyzed by JEM-ARM200F atomic resolution analytical microscope equipped with a STEM Cs corrector operating at 200 kV. The HAADF-STEM images of the precipitates in the peak and over-ageing stage were analyzed by JEM-F200 multi-purpose electron microscope operating at 200 kV. The bright field (BF) and high-resolution transmission electron microscopy (HRTEM) images of the precipitates in the over-ageing stage were analyzed by Tecnai G2 F20-TWIN transmission electron microscope operating at 200 kV.

3 Results and discussion

3.1 Ageing hardness

The age-hardening curve of the Mg−7Gd−3Y−1Nd−1Zn−0.5Zr alloy at 240 °C is shown in Fig. 1. The Brinell hardness value of as-homogenized alloy is about 78, and it increases rapidly in the under-ageing stage. After 18 h of ageing, the Brinell hardness reaches its peak value of 106 which is increased by 35.9% compared with that of the as-homogenized alloy. The hardness plateau can be observed between 18 and 500 h ageing, which shows excellent thermal stability of the alloy. The change of ageing hardness, in fact, mainly depends on the ageing precipitation behavior of α-Mg (S.S.S.S.). In order to further understand the precipitation behavior in ageing stage, the microstructures of the alloy were analyzed.

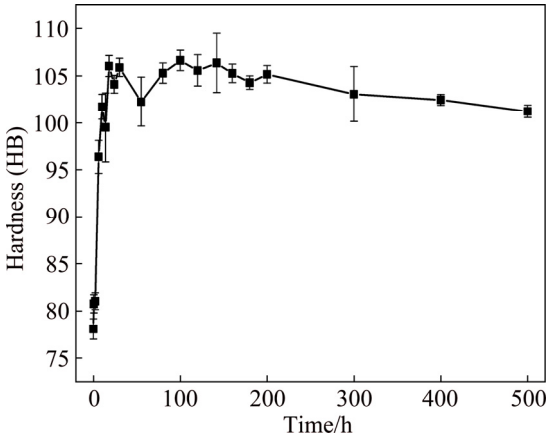

Fig. 1 Age hardening curve of Mg−7Gd−3Y−1Nd− 1Zn−0.5Zr alloy at 240 °C

3.2 Microstructures of aged alloys

3.2.1 Ageing at 240 °C for 2 h

In the under-ageing stage, in order to determine the arrangement of RE atoms in the alloy aged at 240 °C for 2 h, the HAADF-STEM technique was applied. Based on the Z-contrast principle in HAADF imaging and the fact that RE is the heaviest element in the structure [12], we can associate the bright dots to RE atomic column.

Figure 2 shows the HAADF-STEM images and corresponding fast Fourier transform (FFT) of the alloy aged at 240 ºC for 2 h, and the incident electron beam is parallel to the $[0001]_\alpha$ and $[11\bar{2}0]_\alpha$ zone axis. The hexagonal ring structure precipitates (marked by red dotted circle), zigzag plates (marked by yellow dotted circle) and the FFT (located in the upper right corner) are shown in Fig. 2(a). The hexagonal ring structure contains six bright dots, which represent RE-rich columns. All of

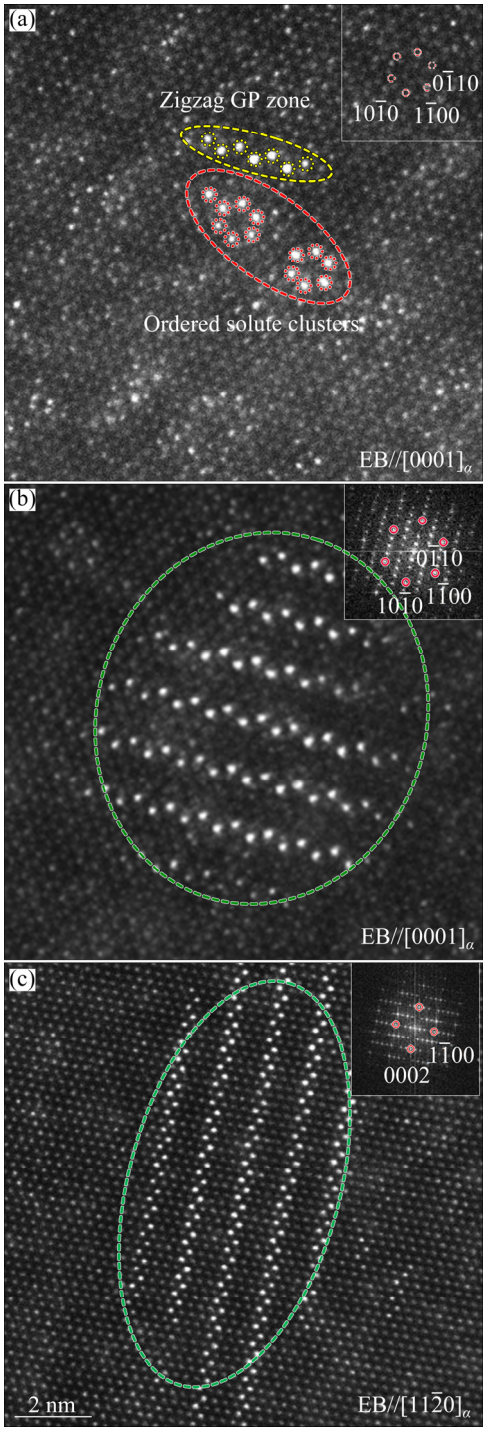

Fig. 2 High resolution HAADF-STEM images: (a) Ordered solute clusters and zigzag GP zone viewed along $[0001]_\alpha$; (b) β' in its early formation viewed along $[0001]_\alpha$; (c) β' in its early formation viewed along $[11\bar{2}0]_\alpha$

these short-range ordered structures can be classified as ordered solute clusters and have been reported in the Mg−Nd and Mg−Y alloys [19]. The ordered solute clusters and zigzag plates form in the habit plane $\{1\bar{1}00\}_\alpha$. These zigzag plates are considered to be prismatic GP zones, as reported in Ref. [19]. The age-hardening behavior in the under-ageing stage shown in Fig. 1 can be attributed to the short-range ordered solute clusters and GP zones. Considering that the content of RE in the present alloy is sufficiently high and the solubility of RE decreases as the temperature decreases, it is assumed that such a large super-saturation can provide sufficient driving force for the formation of hexagonal ring clusters. It can be considered that the zigzag GP zones act as the so-called building blocks in the evolution of β'.

Many zigzag arrays (marked by green dotted circle) and the FFT (located in the upper right corner) are shown in Figs. 2(b) and (c). The two zigzag arrays are separated from each other by a distance of ~1.1 nm, which is equal to the distance in the β' precipitate. Besides, the apexes of the two zigzag arrays are in the opposite directions viewed along $[0001]_\alpha$, as shown in Fig. 2(b), and in the same direction viewed along $[11\bar{2}0]_\alpha$, as shown in Fig. 2(c), which is same as that of the neighboring zigzag arrays in the β' precipitate. Therefore, the zigzag arrays observed in Figs. 2(b) and (c) are more likely to be the β' precipitates in its early formation.

3.2.2 Ageing at 240 °C for 18 h

Figure 3 shows the HAADF-STEM and BF images of the alloy aged at 240 ºC for 18 h, and the incident electron beam is parallel to the $[0001]_\alpha$ and $[11\bar{2}0]_\alpha$ zone axis. The bamboo leaf precipitates marked by the green arrow and the new rod-like precipitates marked by the red arrow are present in the HAADF-STEM image shown in Fig. 3(a). The selected area electron diffraction (SAED) pattern contributed by precipitates shown in Fig. 3(a) (located in the upper right corner) can be indexed as BCO structure with lattice parameters of a=0.64 nm, b=2.22 nm and c=0.52 nm, which is similar to the metastable precipitates β' in other Mg−Gd alloys [20]. Therefore, the metastable precipitates in the peak-ageing stage are also referred to as β' [17]. Figure 3(b) shows the simulated electron diffraction pattern of the three variants of the β' precipitates overlapping the matrix along $[0001]_\alpha$. Both the brighter diffraction spots of the matrix and the weaker spots of the three variants for the β' precipitates exhibit threefold symmetry characteristic in Fig. 3(a). It can also explain that their rotation axis is parallel in the form of $[001]_{\beta'}//[0001]_\alpha$. The orientation relationship between β' precipitates and α-Mg is $(100)_{\beta'}//(11\bar{2}0)_\alpha$ and $[001]_{\beta'}//[0001]_\alpha$. Therefore, three variants are present as shown in Fig. 3(a) with habit planes of $(11\bar{2}0)_\alpha$, $(1\bar{2}10)_\alpha$ and $(2\bar{1}\bar{1}0)_\alpha$, respectively. The β' precipitates have the length of about 4−9 nm along the $\langle 11\bar{2}0\rangle_\alpha$ and about 5−13 nm along $\langle 10\bar{1}0\rangle_\alpha$ when being viewed along $[0001]_\alpha$, as shown in Fig. 3(a). Besides, the ratio of the length in the $\langle 1\bar{1}00\rangle_\alpha$ to the width in the $\langle 11\bar{2}0\rangle_\alpha$ is smaller than that of β' in the EW75 alloy [17].

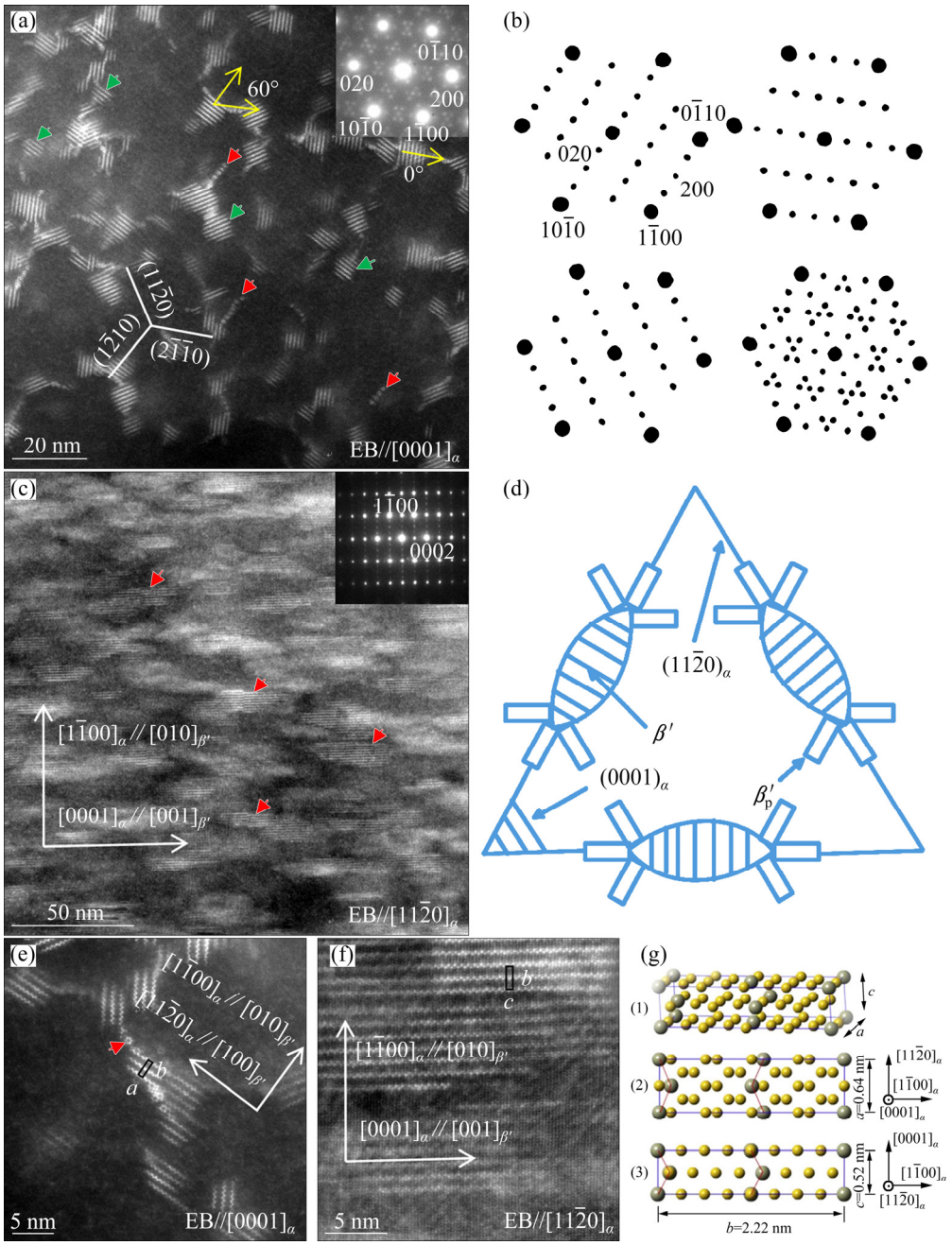

Fig. 3 HAADF-STEM images of alloy aged at 240 °C for 18 h: (a) HADDF-STEM image viewed along $[0001]_\alpha$; (b) Simulated electron diffraction pattern of three variants of β' precipitate and matrix viewed along $[0001]_\alpha$; (c) HAADF-STEM image viewed along $[11\bar{2}0]_\alpha$; (d) Schematic diagram of β' and β'_p in $(0001)_\alpha$; (e) High resolution HADDF-STEM image viewed along $[0001]_\alpha$; (f) High resolution HADDF-STEM image viewed along $[11\bar{2}0]_\alpha$; (g) Structural model of β' precipitate (1), atomic arrangement observed from *c*-axis corresponding to Fig. 3(e) (2) and atomic arrangement observed from *a*-axis corresponding to Fig. 3(f) (3) [17]

Meanwhile, many rod-like precipitates are found next to the β' precipitates, which were not found in our previous studies in the EW75 alloy [17]. To distinguish new rod-like precipitate from subsequent precipitates, it is referred to as β'_p. The β'_p is about 4−7 nm along $\langle 1\bar{1}00\rangle_\alpha$ and 1−2 nm along $\langle 11\bar{2}0\rangle_\alpha$ viewed along the $[0001]_\alpha$, as shown in Fig. 3(a). The angle between the direction of elongation of the β'_p and the direction of $\langle 1\bar{1}00\rangle_\alpha$ is approximately 0° or 60°, as marked by the yellow arrows. The habit plane of the β'_p is $\{11\bar{2}0\}_\alpha$ consistent with that of β'. Meanwhile, it is also found in Fig. 3(e) that the RE atomic columns are arranged in hexagonal rings in the β'_p, as marked by the red arrow. It can be assumed that the β'_p induced by the addition of Zn may be the precursor of β'.

β' precipitates also appear in bamboo leaf shape when being viewed along $[11\bar{2}0]_\alpha$, as shown in Fig. 3(c), which have length of about 19−44 nm along

the $[0001]_\alpha$ and about 5−13 nm along $\langle 1\bar{1}00\rangle_\alpha$. Therefore, based on the observation of the β' precipitates in the two directions of $[0001]_\alpha$ and $[11\bar{2}0]_\alpha$, it can be sure that the precipitate has three-dimensional convex len shape. Figure 3(d) shows the schematic diagram exhibiting the orientation relationship of β' and β'_p precipitates distributing in $(0001)_\alpha$ plane.

In order to describe the crystal structure of the β' precipitate, the *a*-axis is parallel to $[100]_{\beta'}$, *b*-axis is parallel to $[010]_{\beta'}$ and *c*-axis is parallel to $[001]_{\beta'}$. The rectangle marked in the HAADF-STEM image as shown in Fig. 3(e) is a unit cell of β'. The RE atoms in the β' viewed along $[0001]_\alpha$ is zigzag arranged along the $[11\bar{2}0]_\alpha$ (*a*-axis). The rectangle marked in the HAADF-STEM image as shown in Fig. 3(f) is also a unit cell of β' viewed along $[11\bar{2}0]_\alpha$. The RE atoms in the β' viewed along $[11\bar{2}0]_\alpha$ is also zigzag arranged along the $[0001]_\alpha$ (*c*-axis).

As shown in Figs. 3(e) and (f), the structure model of the β' precipitate can be derived as Fig. 3(g). RE atoms are arranged with face-centred symmetry in z=0 and z=1/2 planes, as shown in Fig. 3(g(1)). Based on the present model shown in Fig. 3(g(2)), the atomic arrangement viewed along the *c*-axis, with zigzag arrays of RE atoms along the *a*-axis (marked by red lines) corresponding to the bright dots is shown in Fig. 3(e). Similarly, as shown in Fig. 3(g(3)), the atomic arrangement viewed along the *a*-axis, with zigzag arrays of RE atoms along the *c*-axis (marked by red lines) corresponding to the bright dots is shown in Fig. 3(f). The present structure model of Mg_7RE is similar to the model previously proposed by KARIMZADEH [21], and NISHIJIMA and HIRAGA [22] in Mg−5%Gd and Mg−2%Y alloys. The formation of β' is accomplished by ordered stacking of zigzag GP zones along $\langle 10\bar{1}0\rangle_\alpha$. In the Mg−7Gd−3Y−1Nd−1Zn−0.5Zr alloy, the HAADF-STEM images of the β' precipitates viewed along $[0001]_\alpha$ and $[11\bar{2}0]_\alpha$ prove that the structural model is Mg_7RE. It is obvious that β' and β'_p have different crystal structures.

3.2.3 Ageing at 240 °C for 100 h

Figure 4 shows the SAED pattern, HRTEM and HAADF-STEM images of the alloy aged at 240 °C for 100 h viewed along $[0001]_\alpha$. Two types of precipitates are present in the BF and HAADF-STEM images, as shown in Fig. 4(a) and Fig. 4(b), respectively. The SAED pattern shown in Fig. 4(c) is consistent with that in Fig. 3(a), indicating that most of the precipitates in the over-ageing stage are still metastable β' as marked by red arrows. Since its number is less than that of the β' precipitates, there are no diffraction spots corresponding to the parallelogram precipitates. The FFT corresponding to HRTEM and HAADF-STEM images for these precipitates as shown in Figs. 4(d) and (e) can be indexed as FCC structure with lattice parameters of a=0.74 nm and $d\{11\bar{1}\}_{\beta 1}$=0.43 nm, which are similar to those of the metastable precipitates β_1 in Mg−Y−Nd alloy [23]. The orientation relationship of β_1, β' and α-Mg is $(11\bar{1})_{\beta 1}$ //$(100)_{\beta'}$ // $(11\bar{2}0)_\alpha$ and $[1\bar{1}0]_{\beta 1}$ //$[001]_{\beta'}$ //$[0001]_\alpha$ based on the SAED and FFT patterns. The β' is coherent with the matrix, while the β_1 is not coherent with the matrix.

β' precipitates still appear in bamboo leaf shape when being viewed along $[0001]_\alpha$, as shown in Fig. 4(a), with the length of about 11−19 nm along the $\langle 11\bar{2}0\rangle_\alpha$ and 14−24 nm along $\langle 10\bar{1}0\rangle_\alpha$. The β' precipitates are coarser when the sample is aged at 240 °C for 100 h than 18 h, but the orientation relationship with the matrix does not change. β_1 precipitates with the habit plane of $\{1\bar{1}00\}_\alpha$ appear in parallelogram shape when being viewed along $[0001]_\alpha$, as shown in Fig. 4(a), with the length of about 4−6 nm along $\langle 1\bar{1}00\rangle_\alpha$ and about 14−30 nm along $\langle 11\bar{2}0\rangle_\alpha$. Six variants are identified, as marked by yellow arrows in Fig. 4(a), which are consistent with β_1 proposed by NIE and MUDDLE [23]. Meanwhile, the β'_p found at ageing for 18 h is not found for 100 h. The orietation relationship of three β' and six β_1 variants is shown in Fig. 4(f).

The RE elements are enriched in the β' and the β_1 precipitates when being viewed along $[0001]_\alpha$, as shown in Fig. 4(b). The β_1 precipitates are brighter than the β' precipitates (Mg_7RE), indicating higher RE content in β_1, which is similar to β_1 (Mg_3X) in Mg−Y−Nd alloy [23]. The rectangle marked in the HAADF-STEM image, as shown in Fig. 4(e), is a unit cell of β' precipitate. The RE atoms in the β' precipitate viewed along $[0001]_\alpha$ is zigzag arranged along the $[11\bar{2}0]_\alpha$ (*a*-axis).

The formation of the β_1 precipitate is related to the β' precipitate, because the β_1 precipitate is always connected to two β' precipitates. NIE and MUDDLE [23] believed that due to the existence of shear strain, β_1 may co-nucleate with β' via an invariant plane strain transformation of the magnesium lattice. In contrast, APPS et al [24] believed that both β_1 and β' nucleate on the β'', and the β_1 and β' grow together during the aging process, resulting in the β_1 precipitate always being connected to the two β' precipitates. However, the β'' precipitates are absent in the Mg−7Gd−3Y−1Nd−1Zn−0.5Zr alloy. Meanwhile, there is evidence that the partial decomposition of the β' is converted into the β_1 and the growth of the β_1 depends on the expense of the β', as shown in Fig. 4(b). The final microstructure is that each β_1 precipitate is connected to two β' precipitates.

Figure 5 shows the HAADF-STEM images and SAED pattern of the alloy aged at 240 °C for 100 h viewed along $[11\bar{2}0]_\alpha$. The RE elements are enriched in the β' precipitates, as marked by red arrow, the β_1 precipitates are marked by yellow arrow and the LPSO precipitates are marked by black arrows. When being

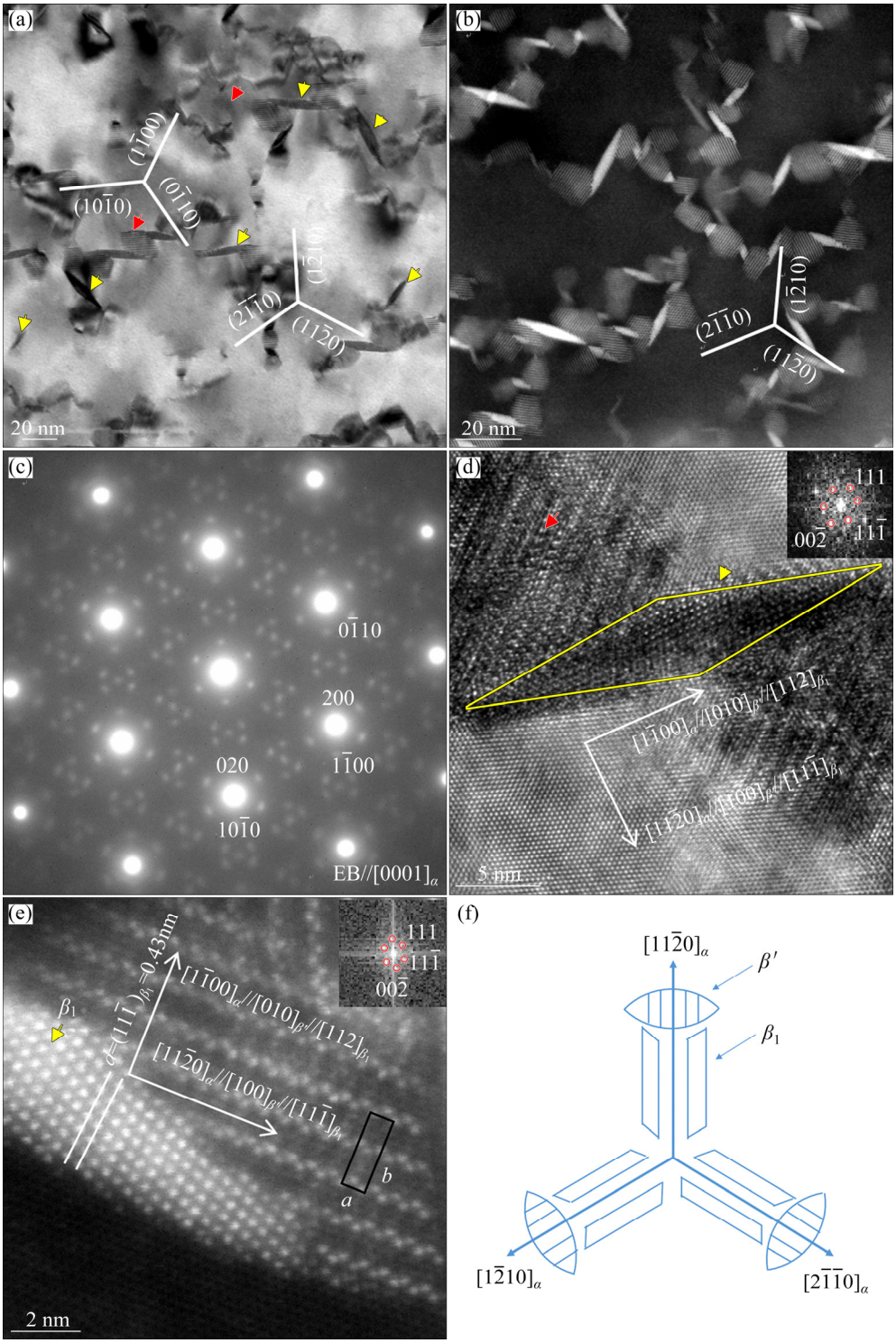

Fig. 4 SAED pattern, HRTEM and HADDF-STEM images of alloy aged at 240 °C for 100 h viewed along $[0001]_\alpha$: (a) BF image; (b) HADDF-STEM image; (c) SAED image; (d) HRTEM image; (e) High resolution HADDF-STEM image; (f) Schematic diagram of realationship of three β' and six β_1 variants

viewed along $[11\bar{2}0]_\alpha$ in Fig. 5(a), β' and β_1 are uniformly distributed in the matrix, but LPSO is not.

β' precipitates also appear in bamboo leaf shape and β_1 precipitates appear in long strip-like shape when being viewed along $[11\bar{2}0]_\alpha$, as shown in Fig. 5(b). The lengths of β' and β_1 in the $[0001]_\alpha$ are about 88−130 nm and 55−120 nm, respectively. It can be known that the size of the β' is larger than that of the β_1. Meanwhile, the LPSO precipitate with the habit plane of $(0001)_\alpha$ has the thickness of about 4 nm along $[0001]_\alpha$. It can be observed in Fig. 5(b) that neither the β_1 nor the β' crosses the LPSO, and the LPSO has a certain hindrance to the

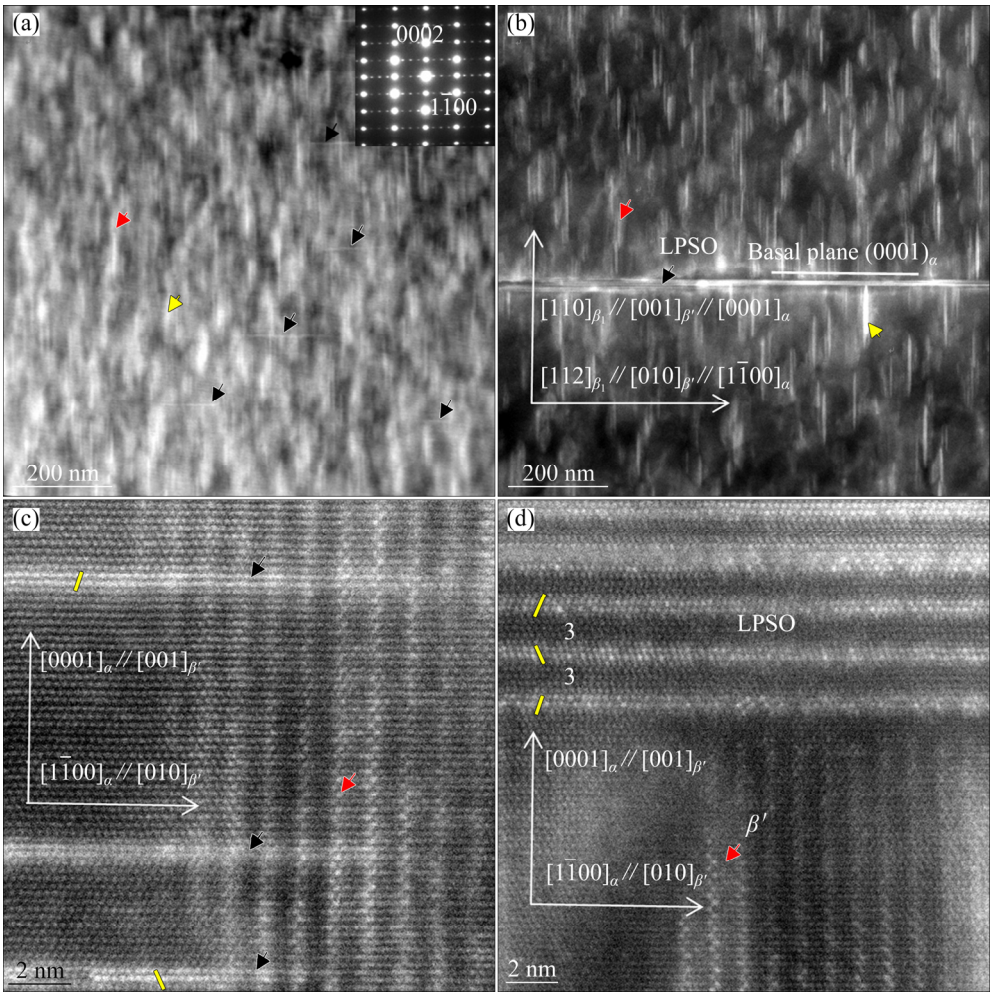

Fig. 5 HAADF-STEM images and SAED pattern of alloy aged at 240 °C for 100 h viewed along $[11\bar{2}0]_\alpha$: (a, b) HAADF-STEM images; (c, d) High resolution HADDF-STEM images

coarsening of the β' and the β_1. It has been proven that the LPSO cannot only effectively retard the grain growth at elevated temperature [25], but also retard the coarsening of β' during ageing [26]. Therefore, we speculate that the LPSO can also retard the coarsening of the β_1.

The stacking sequence of the close-packed plane as marked by the black arrows is "ABCA" and "ACBA", as shown in Fig. 5(c). The precipitates formed on the $(0001)_\alpha$ basal plane are completely coherent with the matrix. These features of the close-packed plane indicate that it is the γ' precipitate that has been reported previously [27,28]. The γ' precipitate is also the building block, which forms the basis of the unit cells of 14H phase as well as 18R phase [28]. The spatial interaction between β' and building blocks retards the coarsening of β' [29].

The stacking sequence of the close-packed plane of each building block is in the opposite direction to that of the neighboring building block, as shown in Fig. 5(d). By combining two neighboring building blocks together, a stacking sequence (ABABCACACACBABA) of the two-dimensional lamellar 14H-LPSO can be obtained. 14H-LPSO is also known as equilibrium γ, as reported in Mg−Gd−Zn, Mg−Y−Zn and Mg−Y−Ag−Zn alloys [11]. The spatial interaction between β' and 14H-LPSO retards the coarsening of β', which is consistent with β' and γ'. The 14H-LPSO has the thickness of about 8 nm along $[0001]_\alpha$.

The γ-type precipitates (γ' or 14H-LPSO) may retard the growth of β' and β_1 along $\langle 0001\rangle_\alpha$ depending on their thickness in $[0001]_\alpha$ direction. The thermal stability of the β' and β_1 is also related to the low diffusion rate of RE atoms or the physical character of the β' and β_1 precipitates. Therefore, we can infer that the 14H-LPSO gradually increases and further retards the coarsening of the β_1 and β', so there is still a higher thermal stability until ageing for 500 h, as shown in Fig. 1.

The schematic diagram for the realationship of the LPSO, β' and β_1 is shown in Fig. 6. With the β' and β_1 strengthening the matrix and the growth of the two kinds of precipitate limited by 14H-LPSO, the alloy possesses

excellent long-term thermal stability at 240 °C. Therefore, the ideal microstructure provides a new idea for the design of the next generation magnesium alloys with excellent mechanical properties over a wide temperature range.

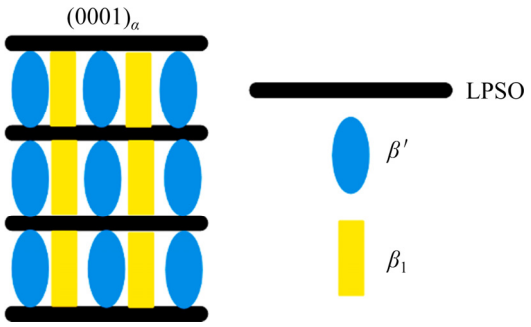

Fig. 6 Schematic diagram of realationship of LPSO, β' and β_1

4 Conclusions

(1) After ageing at 240 °C for 2 h, the precipitates are composed of ordered solute clusters, zigzag GP zones and the β' precipitate in its early formation. The ordered solute clusters and the zigzag GP zones form in the habit plane $\{1\bar{1}00\}_\alpha$. The zigzag GP zones act as the so-called building blocks in the evolution of β'.

(2) After ageing at 240 °C for 18 h, the precipitates are β' and β'_p phases. The structural model of the lenticular β' (BCO, a=0.64 nm, b=2.22 nm and c=0.52 nm) is Mg_7RE-type. The formation of β' is accomplished by ordered stacking of zigzag GP zones along $\langle 10\bar{1}0\rangle_\alpha$. The β'_p has the hexagonal ring structure which is considered as the precursor of β'.

(3) After ageing at 240 °C for 100 h, the precipitates are β', β_1, γ' and 14H-LPSO. β_1 (FCC, a=0.74 nm) is converted from β'. The γ' is the building block of 14H-LPSO.

(4) The alloy shows the excellent thermal stability (18−500 h), which is attributed to the fact that the γ' or 14H-LPSO may retard the growth of β' and β_1 along $[0001]_\alpha$, low diffusion rate of RE atoms and physical character of β' and β_1.

References

[1] WANG X J, XU D K, WU R Z, CHEN X B, PENG Q M, JIN L, XIN Y C, ZHANG Z Q, LIU Y, CHEN X H, CHEN G, DENG K K, WANG H Y. What is going on in magnesium alloys? [J]. Journal of Materials Science and Technology, 2018, 34(2): 245−247.

[2] CHEN Hong-bing, LIU Tian-mo, LU Li-wei, HE Jie-jun, ZHAI Yan-bo. Influence of pre-strain and heat treatment on subsequent deformation behavior of extruded AZ31 Mg alloy [J]. Transactions of Nonferrous Metals Society of China, 2015, 25(11): 3604−3610.

[3] LIU Di, LIU Zu-yan, WANG Er-de. Improving single pass reduction during cold rolling by controlling initial texture of AZ31 magnesium alloy sheet [J]. Transactions of Nonferrous Metals Society of China, 2018, 28(2): 244−250.

[4] MASSALSKI T B, MURRAY J L, BENNETT L H, BAKER H. Binary alloy phase diagrams [M]. Ohio: American Society for Metals, 1986.

[5] PENG Qiu-ming, WANG Jian-li, WU Yao-ming, MENG Jian, WANG Li-min. The effect of La or Ce on ageing response and mechanical properties of cast Mg−Gd−Zr alloys [J]. Materials Characterization, 2008, 59(4): 435−439.

[6] TIAN Zheng, YANG Qiang, GUAN Kai, MENG Jian, CAO Zhan-yi. Microstructure and mechanical properties of a peak-aged Mg−5Y−2.5Nd−1.5Gd−0.5Zr casting alloy [J]. Journal of Alloys and Compounds, 2018, 731: 704−713.

[7] CHEN D J, ZHANG K, LI T, LI X G, LI Y G, MA M L, SHI G L, YUAN J W. Weak strengthening effect of the precipitated lamellar phase in the homogenized Mg−8Gd−4Y−1.6Zn−0.5Zr (wt.%) alloy followed by furnace cooling [J]. Materials Science and Engineering A, 2019, 744: 1−9.

[8] LI Meng, Zhang Kui, DU Zhi-Wei, LI Xing-gang, MA Ming-long. Microstructure evolution and mechanical properties of Mg−7Gd−3Y−1Nd−1Zn−0.5Zr alloy [J]. Transactions of Nonferrous Metals Society of China, 2016, 26(7): 1835−1842.

[9] VOSTRY P, SMOLA B, STULIKOVA I, VONBUCH F, MORDIKE B L. Microstructure evolution in isochronally heat treated Mg−Gd alloys [J]. Physica Status Solidi, 2015, 175(2): 491−500.

[10] GAO X, HE S M, ZENG X Q, PENG L M, DING W J, NIE J F. Microstructure evolution in a Mg−15Gd−0.5Zr (wt.%) alloy during isothermal aging at 250 °C [J]. Materials Science and Engineering A, 2006, 431(1): 322−327.

[11] NIE J F. Precipitation and hardening in magnesium alloys [J]. Metallurgical and Materials Transactions A, 2012, 43(11): 3891−3939.

[12] ZHANG Y, RONG W, WU Y J, PENG L M, NIE J F, BIRBILIS N. A detailed HAADF-STEM study of precipitate evolution in Mg−Gd alloy [J]. Journal of Alloys and Compounds, 2019, 777: 531−543.

[13] LIU Ke, ZHANG Jing-huai, TANG Ding-xiang, ROKHLINC L L, ELKINC F M, MENG Jian. Precipitates formed in a Mg−7Y−4Gd−0.5Zn−0.4Zr alloy during isothermal ageing at 250 °C [J]. Materials Chemistry and Physics, 2009, 117(1): 107−112.

[14] YAMASAKI M, ANAN T, YOSHIMOTO S, KAWAMURA Y. Mechanical properties of warm-extruded Mg–Zn–Gd alloy with coherent 14H long periodic stacking ordered structure precipitate [J]. Scripta Materialia, 2005, 53(7): 799−803.

[15] ANDERSSON P, CACERES C H, KOIKE J. Hall−Petch parameters for tension and compression in cast Mg [J]. Materials Science Forum, 2003, 419: 123−128.

[16] HONMA T, OHKUBO T, KAMADO S, HONO K. Effect of Zn additions on the age-hardening of Mg−2.0Gd−1.2Y−0.2Zr alloys [J]. Acta Materialia, 2007, 55(12): 4137−4150.

[17] LI Ting, DU Zhi-wei, ZHANG Kui, LI Xing-gang, YUAN Jia-wei, LI Yong-jun, MA Ming-long, SHI Guo-liang, FU Xin, HAN Xiao-lei. Characterisation of precipitates in a Mg−7Gd−5Y−1Nd−0.5Zr alloy aged to peak-ageing plateau [J]. Journal of Alloys and Compounds, 2013, 574: 174−180.

[18] LI M, WANG X, FENG Q Y, WANG J, XU Z, ZHANG P H. The effect of morphology of the long-period stacking ordered phase on mechanical properties of the Mg−7Gd−3Y−1Nd−1Zn−0.5Zr (wt.%) alloy [J]. Materials Characterization, 2017, 125: 123−133.

[19] NIE J F, WILSON N C, ZHU Y M, XU Z. Solute clusters and GP zones in binary Mg–RE alloys [J]. Acta Materialia, 2016, 106: 260−271.

[20] ZHANG Yu, ZHU Yu-man, RONG Wei, WU Yu-jun, PENG Li-ming, NIE Jian-feng, BIRBILIS N. On the precipitation in an Ag-containing Mg−Gd−Zr alloy [J]. Metallurgical and Materials Transactions A, 2018, 49(2): 673−694.

[21] KARIMZADEH H. The microstructure and mechanical properties of some magnesium alloys containing yttrium and heavy rare earth [D]. Manchester: Department of Metallurgy, University of Manchester, 1985.

[22] NISHIJIMA M, HIRAGA K. Structural changes of precipitates in an Mg−5at%Gd alloy studied by transmission electron microscopy [J]. Materials Transactions, 2007, 48(1): 10−15.

[23] NIE J F, MUDDLE B C. Characterisation of strengthening precipitate phases in a Mg–Y–Nd alloy [J]. Acta Materialia, 2000, 48(8): 1691−1703.

[24] APPS P J, KARIMZADEH H, KING J F, LORIMER G W. Precipitation reactions in magnesium-rare earth alloys containing yttrium, gadolinium or dysprosium [J]. Scripta Materialia, 2003, 48(8): 1023−1028.

[25] LI Y X, QIU D, RONG Y H, ZHANG M X. Effect of long-period stacking ordered phase on thermal stability of refined grains in Mg−RE-based alloys [J]. Philosophical Magazine, 2014, 94(12): 1311−1326.

[26] LI Y X, ZHU G, QIU D, YIN D D, RONG Y H, ZHANG M X. The intrinsic effect of long period stacking ordered phases on mechanical properties in Mg−RE based alloys [J]. Journal of Alloys and Compounds, 2016, 660: 252−257.

[27] ZHU Y M, OH-ISHI K, WILSON N C, HONO K, MORTON J, NIE J F. Precipitation in a Ag-containing Mg−Y−Zn alloy [J]. Metallurgical and Materials Transactions A, 2016, 47(2): 927−940.

[28] ZHANG Jing-hua, LIU Shu-juan, WU Rui-zhi, HOU Le-gan, ZHANG Mi-lin. Recent developments in high-strength Mg-RE-based alloys: Focusing on Mg−Gd and Mg−Y systems [J]. Journal of Magnesium and Alloys, 2018, 6(3): 277−291.

[29] KIM J K, KO W S, SANDLOBES S, HEIDELMANN M, GRABOWSKI B, RAABE D. The role of metastable LPSO building block clusters in phase transformations of an Mg−Y−Zn alloy [J]. Acta Materialia, 2016, 112: 171−183.

Mg−7Gd−3Y−1Nd−1Zn−0.5Zr 合金在 240 °C 等温时效过程中析出相的演化

刘 伟[1,2]，杜志伟[1,2,3]，李 婷[1,2,3]，张 奎[4]，韩小磊[1,2]，
彭永刚[1,2]，张 婧[1,2]，袁家伟[4]，刘淑凤[1,2]，庞 铮[1,2]

1. 国标(北京)检验认证有限公司，北京 100088；
2. 有研科技集团有限公司 国家有色金属及电子材料分析测试中心，北京 100088；
3. 国合通用测试评价认证股份公司，北京 100088；
4. 有研工程技术研究院有限公司 有色金属材料制备加工国家重点实验室，北京 101407

摘 要：采用 TEM 和 HAADF-STEM 技术，研究 Mg−7Gd−3Y−1Nd−1Zn−0.5Zr 合金在 240 °C 等温时效过程中析出相的形态与晶体学特征。经 2 h 欠时效，析出相为稀土原子柱呈六角环状结构的有序溶质团簇、之字形 GP 区和早期形成的 β'相。经 18 h 峰时效，析出相主要为 β'相和与其伴生的一种新型棒状相 β'_p。经 100 h 过时效，析出相为 β'相、β_1 相、长程堆垛有序(LPSO)构建块 γ'相和 14H-LPSO。β'相三维形貌呈凸透镜状，沿$\langle 0001\rangle_\alpha$方向观察，其长宽比小于 EW75 合金中 β'相的长宽比。该合金优异的热稳定性归功于 γ'和 14H-LPSO 阻碍 β'和 β_1 的生长、稀土原子低的扩散速率以及 β'和 β_1 相的物理特性。

关键词：镁合金；时效；析出相；长程堆垛有序相

(Edited by Bing YANG)